Postprint of: Nykiel G., Figurski M., Baldysz Z., Analysis of GNSS sensed precipitable water vapour and tropospheric gradients during the derecho event in Poland of 11th August 2017, JOURNAL OF ATMOSPHERIC AND SOLAR-TERRESTRIAL PHYSICS, Vol. 193 (2019), 105082, DOI: 10.1016/j.jastp.2019.105082

Analysis of GNSS sensed precipitable water vapour and tropospheric gradients during the derecho event in Poland of 11th August 2017

Grzegorz Nykiel*, Mariusz Figurski, Zofia Baldysz

Faculty of Civil and Environmental Engineering, Gdansk University of Technology, G. Narutowicza 11/12, 80-233, Gdansk, Poland

** Corresponding author.*
E-mail address: grzegorz.nykiel@pg.edu.pl

ABSTRACT

Nowadays, one of the techniques that meets the increasing requirements of meteorologist in terms of monitoring of severe weather events is global navigation satellite systems (GNSS), which can provide information about the tropospheric state independently of the weather conditions and even in real time. In this paper we present the usage of GNSS sensed tropospheric data to monitor sudden and intense weather events. Our analyses were performed on the example of a derecho event in Poland of 11th August 2017. We used GPS/GLONASS observations from 278 GNSS reference stations located in Poland and, using Bernese GNSS Software ver. 5.2, we estimated the zenith tropospheric delays (ZTD) and tropospheric gradients with 5 and 15-min intervals respectively. Next, using meteorological data from the synoptic stations, we estimated the precipitable water vapour (PWV) which gives information about the amount of water vapour in the atmosphere. By applying a dense network of GNSS receivers, we were able to create the PWV, rate of the PWV (ROP), and the tropospheric gradients maps, which in turn allowed us to monitor the derecho event. We also conducted case studies for the selected GNSS stations where a comparison between PWV, reflectivity, and microwave radiometer were performed. During the main phase of the event we obtained the maximum value of PWV equal to 52.1 mm at 20:30 UTC. We also acquired high agreement between the PWV/ROP maps and reflectivity derived from meteorological radars. This applies to both the direction and speed of the phenomena as well as the time and place of the occurrence of the main phase of the derecho. This was possible only owing to the use of data derived from the dense network of the GNSS receivers.

Keywords: GNSS, Precipitable water vapour, PWV/IWV, Severe weather monitoring, Tropospheric gradients, Derecho

1. Introduction

Water vapour in the Earth's atmosphere is extensively studied by climatologists and meteorologists. The reason is simple: water vapour is involved in various processes in a whole range of scales, including energy transport, condensation, cloud formation and precipitation. Therefore, short and long-term changes in weather patterns crucially depend on variability in the content of atmospheric water vapour (Randall, 2000). While its deficiency over some areas may lead to a long-term drought, its increased amount over other areas can lead to more frequent occurrences of extreme weather conditions. Therefore, collection of the information about variability in the water vapour content in the

troposphere is especially important in the era of atmospheric warming, which is inextricably linked to the rise of violent and severe weather events, including rapid and heavy precipitation and storms (Cornwall, 2016; Herring et al., 2018). Moisture content of an atmospheric column, which is inter alia indicated by precipitable water vapour (PWV), can be theoretically derived by calculating the amount of liquid water resulting from condensation of all water vapour from the Earth's surface to the top of the atmosphere. Similarly, as rainfall, PWV is measured in millimetres. A high PWV value is favourable for heavy rainfall or storm. Therefore, PWV monitoring is helpful in identifying moisture sources and analysing the development and evolution of weather systems, including those related to a storm cell formations (Benevides et al., 2015).

There are two traditional techniques of measuring PWV from the Earth's surface, namely, radiosondes and microwave radiometers (MWR). Both these techniques have some limitations that make collecting PWV data with high spatial and temporal resolution difficult. Radiosondes measurements are performed usually only twice a day (up to four times a day) using a meteorological balloon. They are characterised by an instrument drift ranging about 20–50 km depending on the wind direction and speed (Seidel et al., 2011). Moreover, this technique requires free airspace during the launch, and a balloon ascends, which is hindered over an urbanised area due to high air traffic. Furthermore, spatial resolution of a radio sounding stations is low and insufficient for the monitoring of rapid changes in the troposphere. On the other hand, microwave measurements require expensive equipment and are very sensitive to weather conditions. The data quality is optimal during clear sky conditions or when a base of clouds is above the atmospheric boundary layer, because they strongly suppress microwaves. However, an unquestionable advantage of this technique lies in the possibility to estimate a condition within troposphere not only directly over MWR itself but also in the immediate surroundings of the station by scanning along various azimuthal and angular angles. However, the spatial distribution of MWR stations is very low, mainly due to the high cost of the instrument. In the past 20 years, another remote sensing method to obtain PWV based on signals from global navigation satellite system (GNSS) has been developed. This approach employs a certain feature of the GNSS, namely, a requirement to estimate the so-called zenith tropospheric delay (ZTD) parameter during precise positioning. The ZTD is a combination of two parameters: zenith hydrostatic delay (ZHD) and zenith wet delay (ZWD). They are determined by meteorological parameters such as air pressure and temperature (ZHD), and humidity (ZWD). As a result, ZTD reflects the instantaneous state of the troposphere, while its variability indicates changes in weather. ZTD can be directly converted to the PWV (Bevis et al., 1992) which allows using the GNSS technique both in climate (Nilsson and Elgered, 2008; Ning and Elgered, 2012; Baldysz et al., 2016, 2017) and meteorological studies (Gradinarsky et al., 2002; Pacione et al., 2001; Faccani et al., 2005; Guerova et al., 2016). A very high temporal and spatial resolution of GNSS data makes it possible to use GNSS in severe weather phenomena analyses such as typhoon (Zhao et al., 2018), heavy precipitations (Seko et al., 2000; Zhang et al., 2007) or storms (Choy et al., 2013). The meteorological application of GNSS includes also nowcasting of severe weather events. The prediction of lightening (Mazany et al., 2002; Kehrer et al., 2008; Suparta and Ali, 2014) or heavy precipitations (Vedel et al., 2004; Benevides et al., 2015; Qingzhi et al., 2018) have been performed using this approach.

Based on previous analyses it can be stated that the GNSS technique has both advantages and disadvantages. The main shortcomings include: (a) complicated estimation methods, (b) dependence of the results on the quality of the external precise products, especially in the absolute precise point positioning (PPP) method, (c)

imperfection of the used methodology, especially in the case of slant tropospheric delays, (d) a lack of tropospheric profiles (directly), (e) a maximum 24-year time span of observations (limited to some stations of International GNSS Service (IGS)), and (f) a strong dependence of results on the station equipment and the discontinuities caused by equipment changes. The last two drawbacks apply only when using GNSS data for climate analyses. For the purpose of monitoring severe weather events, they are practically irrelevant. Due to the progress in the methodology of GNSS observations processing, the development of precise products and new algorithms, the remaining four disadvantages cease to play a significant role. At the same time, the advantages of GNSS techniques are becoming increasingly important. The main benefits include: (a) high temporal resolution of the tropospheric delay estimation (even less than a second), (b) independence of weather conditions, (c) the fact that the GNSS signal goes through the whole troposphere, and (d) continuous increase of spatial resolution of the estimated tropospheric parameters along with the densification of the GNSS infrastructure.

Owing to the unquestionable advantages of the GNSS technique, PWV has been established as a possibly valuable element of warning systems for severe weather events (Brenot et al., 2013). These warnings against severe weather phenomena start to take on a greater significance, since such unusual natural hazards become increasingly common (Field et al., 2012). One of these rapid and extremely dangerous weather events is derecho. This specific storm is characterised by very strong, gusty straight-line winds that occur in a widespread area (up to hundreds of kilometres). It is associated with several simultaneously moving mesoscale convective systems. It often takes a bow echo form, carries a high risk of extreme damage and is life-threatening. Such an event is also associated with a temporary and very intense rainfall, storm or even hail. Traditional ground-based meteorological measurements (synoptic and sounding) are insufficient in the monitoring of such rapid and intense events. This does not apply to meteorological radars that give information on reflectivity in the atmosphere caused by hydrometeors. The magnitude of the reflectivity provides data about the type and the quantity of hydrometeors. However, obtaining such information is not easy and requires experience in processing and interpreting radar measurements. Moreover, meteorological radars are not without disadvantages. Radar users usually mention the following necessary improvements: better spatial and temporal resolution, better reliability, consistent and low-altitude information, as well as detection of precipitation type, size and intensity in single polarisation radars (LaDue et al., 2009).

The solution for some of the mentioned disadvantages may be the application of GNSS PWV, especially obtained from the dense network of receivers, which can provide reliable data with high temporal resolution. The usage of a large number of GNSS stations allows a PWV map to be obtained, which can be successfully employed in weather monitoring, separately or together with other meteorological data. In this paper, we present the possibility of monitoring a severe weather event using dense GNSS networks in Poland. Our analyses were performed for the case study of a derecho that took place on 11th August 2017. First, we provide short information about the event with visualisation based on composite radar measurements. In Section 3, we introduce GNSS data as well as the methodology necessary to obtain reliable PWV values. Next, in Results we present maps of PWV and the rate of PWV including accuracy and reliability assessments. We also show maps of tropospheric delay gradients and their possible application in the monitoring of severe weather events. Moreover, we present two case study examples for the selected GNSS stations with a comparison to the radar measurements. Lastly, we provide some discussion on the obtained results, conclusions and recommendations.

Postprint of: Nykiel G., Figurski M., Baldysz Z., Analysis of GNSS sensed precipitable water vapour and tropospheric gradients during the derecho event in Poland of 11th August 2017, JOURNAL OF ATMOSPHERIC AND SOLAR-TERRESTRIAL PHYSICS, Vol. 193 (2019), 105082, DOI: 10.1016/j.jastp.2019.105082

2. Derecho in Poland, 11th August 2017

A severe storm event analysed in this paper passed over Poland on 11–12th August 2017. The formation of this dangerous phenomenon later classified as derecho (Widawski and Pilorz, 2018), began in the afternoon on 11th August, when initial cloud clusters and thunderstorms formed over the Czech Republic. The weather system moved northward, while convective cells embedded in this system started to intensify over the territory of Poland. At the same time a several so called training storms occurred in south-western Poland, causing a significant increase in humidity over the area. High humidity combined with high temperature resulting from the clear sky conditions caused a destabilisation of the atmosphere and created favourable conditions for a formation of a strong convection on the path of the weather system approaching from the south. As a result, the convective cells re-emerged around 14:00 UTC. Over time, more convective cells developed and began to merge with each other and the system approaching from the south. As a result of this aggregation, a mesoscale convective was formed and this system grew and evolved while moving north northeast. Around 18:00 UTC convective cells embedded in the system formed a squall line. Before 19:00 UTC, as a result of strong descending currents, a visible bow-echo structure was formed and started to move north with the propagation velocity of about 90 km/h, continuously growing stronger. Its maximum activity was observed just after 20:00 UTC and occurred over the northern Poland. At that time, the bow echo structure was about 150 km long. Due to the high velocity of this thunderstorms system, its most dangerous part was preceded by a wind burst that preceded the squall line by two to three minutes. The wind speed reached 120 km/h in gusts and in some places exceeded 150 km/h (Elblag-Milejowo synoptic station). Numerous lightnings were also recorded. The system was moving north over the next three hours and left the territory of Poland soon after 01:00 UTC. Results of this violent weather system involved wind damages over a swath of over 400 km, including a loss of 72,000 ha of agricultural crops and 45,000 ha of wind-fallen trees. Over 500,000 households were deprived of electricity, whereas structural damage to buildings was estimated at about 58 million euro. There were also several fatalities. It has been the strongest derecho in Poland since 2002 (Widawski and Pilorz, 2018). Fig. 1 shows the reflectivity with a 2 km spatial resolution over the study area for the period from 16:30 to 22:00 UTC in 30-minute steps. It depicts the size, shape, propagation velocity and intensity of the derecho. During the main phase of this event, the maximum reflectivity was over 70 dBZ, which indicates a likely presence of extremely heavy precipitation with possible hail.

To provide a better overview of the synoptic situation during the event, Fig. 2 presents selected meteorological parameters derived from the numerical simulations. These were conducted using Weather Research and Forecasting Model (WRF) ver. 4.0.1 (Powers et al., 2017) with the ERA5 reanalysis model (Copernicus Climate Change Service (C3S), 2017) as an initial and boundary conditions. High spatial resolution of the model (2.5 km) depicts well the mesoscale structures in the distribution of the parameters such as surface temperature and sea level pressure, as well as synoptic scale conditions in which the weather system develops and evolves. It can be seen that the derecho occurred on the edge of cold air masses that were advected to Poland from the southwest. The inflow of very cold air over the heated surface (temperature difference up to 20 degrees) supported destabilisation of the troposphere and favoured development of a very strong convection.

Postprint of: Nykiel G., Figurski M., Baldysz Z., Analysis of GNSS sensed precipitable water vapour and tropospheric gradients during the derecho event in Poland of 11th August 2017, JOURNAL OF ATMOSPHERIC AND SOLAR-TERRESTRIAL PHYSICS, Vol. 193 (2019), 105082, DOI: 10.1016/j.jastp.2019.105082

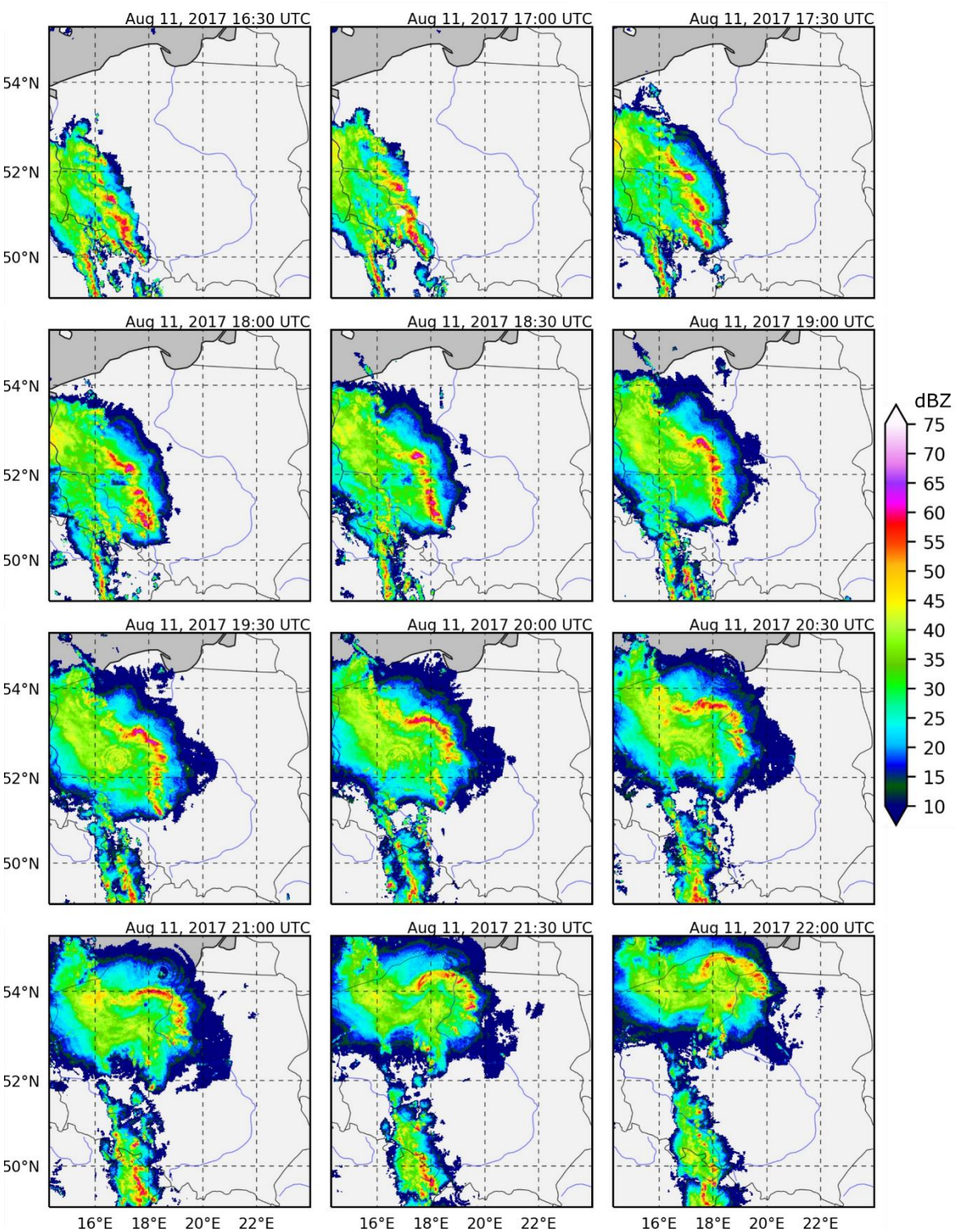

Fig. 1. Composite reflectivity data over the study area on 11th August 2017. Data with 2-km spatial resolution presented from 16:30 to 22:00 UTC in 30-minute steps. Data provided by EIG EUMETNET.

Postprint of: Nykiel G., Figurski M., Baldysz Z., Analysis of GNSS sensed precipitable water vapour and tropospheric gradients during the derecho event in Poland of 11th August 2017, JOURNAL OF ATMOSPHERIC AND SOLAR-TERRESTRIAL PHYSICS, Vol. 193 (2019), 105082, DOI: 10.1016/j.jastp.2019.105082

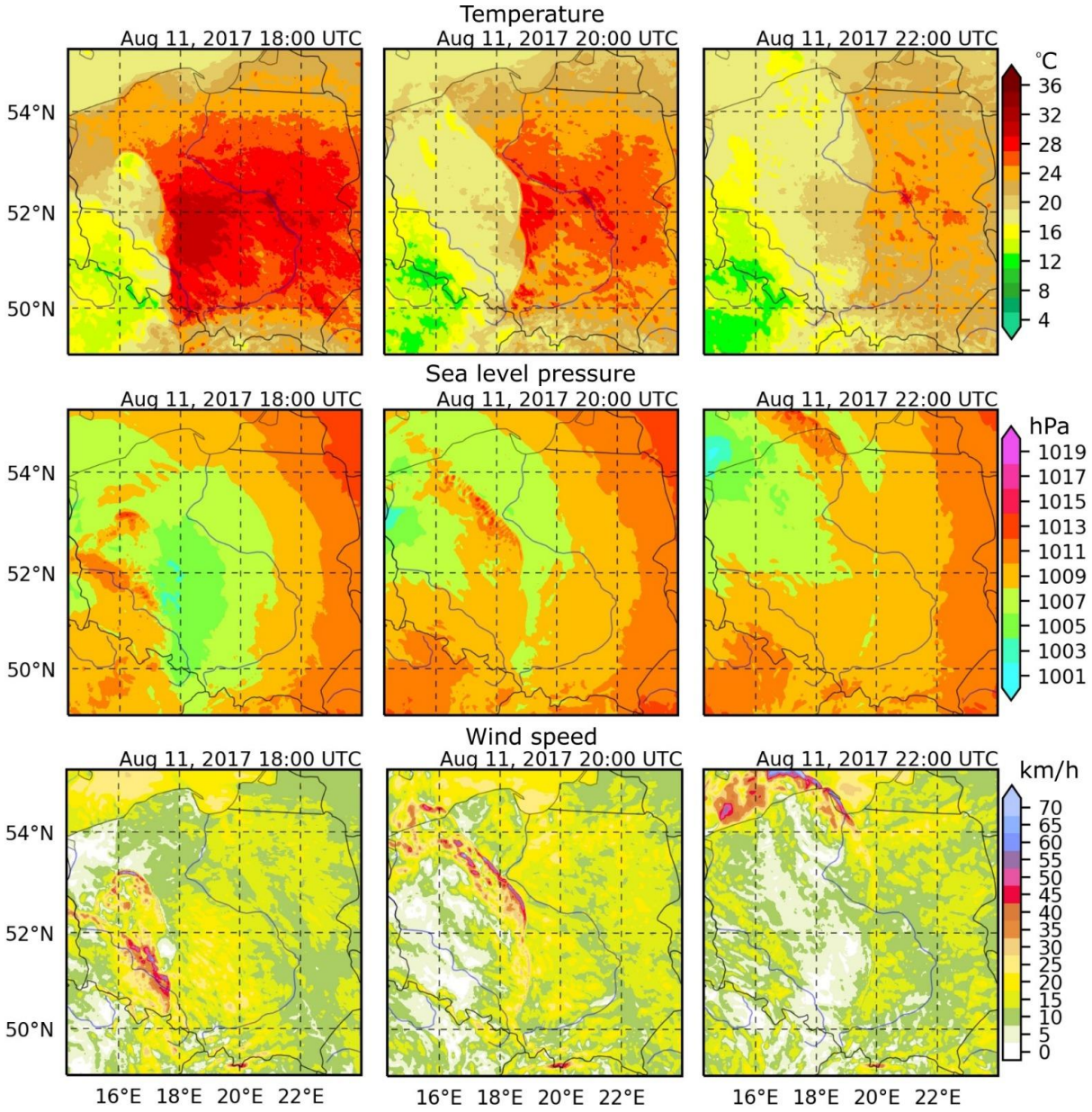

Fig. 2. Map of temperature at 2 m (top), sea level pressure (middle), and wind speed at 10 m (bottom) over the study area on 11th August 2017. Instantaneous fields during the event are presented: 18:00 UTC (left), 20:00 UTC (centre), 22:00 UTC (right). Results obtained from numerical simulations using WRF model.

3. Methodology and data

PWV Estimation. Radio waves passing through the Earth's atmosphere are delayed by free electrons in the ionosphere and temperature, pressure and water vapour in the troposphere. In our study, we consider only the tropospheric delay (T) which is caused by the refraction of the signal. In general, this delay can be defined by the following formula (Bevis et al., 1992):

$$T = c\tau = 10^{-6} \int_0^\infty N(s)ds \quad (1)$$

where c is the speed of light in the vacuum, τ is the delay measured in the unit of time and N is the neutral atmospheric refractivity consisting of hydrostatic and wet parts (Davis et al., 1985):

$$N = N_{hyd} + N_{wet} = K_1(P - e) + K_2\frac{e}{T} + K_3\frac{e}{T^2} \tag{2}$$

where T is the temperature in [K], P is the total air pressure in [hPa], e is the water vapour pressure in [hPa], and K_1, K_2, K_3 are the air refractivity parameters.

Many studies decompose the ZTD parameter (often used interchangeably with the "zenith path delay" abbreviated as ZPD), representing total tropospheric delay in the zenith direction, into:

$$ZTD = ZHD + ZWD \tag{3}$$

where ZHD represents the zenith hydrostatic delay and ZWD is the zenith wet delay. ZTD is a direct product of GNSS processing and can be expressed as follows:

$$\begin{aligned} ZTD &= ZHD + ZWD \\ &= mf_h(el) \cdot SHD + mf_w(el) \cdot SWD + mf_g(G_N \cos(\alpha) + G_E \sin(\alpha)) \end{aligned} \tag{4}$$

where SHD and SWD are slant delays in the direction to a satellite for the hydrostatic and wet tropospheric delays, respectively. They are projected on the zenith direction using the corresponding mapping functions: mf_h and mf_w. Their values strongly depend on the satellite elevation angle (el) and can be obtained using the following equation (Herring et al., 1992):

$$mf(el) = \frac{1 + \dfrac{a}{1 + \dfrac{b}{1 + c}}}{\sin(el) + \dfrac{a}{\sin(el) + \dfrac{b}{\sin(el) + c}}} \tag{5}$$

where a, b, c are coefficients of hydrostatic or wet delays. In modern GNSS processing these coefficients mainly come from two sources: the Vienna Mapping Function 1 (VMF1) (Boehm et al., 2006b) or the Global Mapping Function (GMF) (Boehm et al., 2006a). In Eq. (4) G_N and G_E denote azimuth (α) dependent gradients, defined relative to the north and east directions, while mf_g is the gradient mapping function. In this study the Chen and Herring gradient mapping function (Chen and Herring, 1997) was used.

ZTD, together with the position, is a direct product from processing. However, from the point of view of meteorological and climate application, the more important parameter is ZWD which is strongly correlated with an atmospheric water vapour content. In order to extract its value from Eq. (3), one has to know the ZHD value. If meteorological observations from nearby sounding station or data from a numerical weather model are available, the ZHD can be expressed by the following integral along an atmospheric profile:

$$ZHD = 10^{-6}\int_{h_0}^{\infty} K_1\frac{P - e}{T}dh \tag{6}$$

Otherwise, surface meteorological parameters and approximated, yet rather accurate, Saastamoinen hydrostatic model (Saastamoinen, 1972; Bevis et al., 1994) can be used:

$$ZHD = \frac{0.0022767 * P}{1 - 0.0026 * \cos 2\varphi - 0.00000028 * h} \tag{7}$$

where φ is the ellipsoidal latitude, and h is the height above the ellipsoid [m].

Once ZHD is known, it can be used to extract ZWD from GNSS provided ZTD. ZWD can be analysed separately as an indicator of an amount of the water vapour in the troposphere. It can also be converted to PWV (or integrated water vapour, IWV) to provide a more useful information in meteorological and climatological applications. The conversion to IWV $[kg \cdot m^{-2}]$ can be performed using the following formula:

$$IWV = \Pi(T_m) \cdot ZWD \tag{8}$$

$\Pi(Tm)$ is a dimensionless quantity dependent on the mean weighted temperature of the atmosphere (Tm):

$$\Pi^{-1} = 10^{-8}\left(R_v * (K_3 T_m + K_2')\right) \tag{9}$$

where R_v is the specific gas constant of water vapour and equals to 461.5 J/kg K, and:

$$K_2' = K_2 - K_1 \frac{M_w}{M_d} \approx 22.1\ [K/hPa] \tag{10}$$

K_1, K_2, K_3 are the air refractivity parameters. We used the "best average" values estimated by Ruger (2002) and equal to 77.689 ± 0.0094 K/hPa, 71.295 ± 1.3 K/hPa, and 3.75463e5 ± 0.0076 K2/hPa respectively. M_d = 28.9644, and M_w = 18.0151 are the molar masses of dry and wet air [g/mol].

The PWV, expressed in millimetres, is a IWV scaled by the density of water (ρ):

$$PWV = IWV/\rho \tag{11}$$

As a principal, T_m is obtained by vertical integration of the temperature and water vapour pressure in the atmosphere. However, as we mentioned before, it requires a sounding station, microwave radiometer (MWR) or data from an accurate and validated numerical weather model near a GNSS station. If such data are not available, a linear relationship between T_m and the surface temperature (T_s) may be used. One of the most popular relationships was proposed by Bevis et al. (1994):

$$T_m = 0.72T_S + 70.2 \tag{12}$$

This formula allows estimation of T_m with the root mean square (RMS) error of 4.74 K. It should be mentioned that the 1 K error of the T_m gives 0.40–0.32% error of Π (for the T_m between 250–310 K, typical range for Earth's troposphere), which translates into the 0.05–0.17 mm error of PWV (for the ZWD between 0.1–0.3 m, typical range for Polish area).

To obtain PWV from GNSS, one should employ the processing of two surface meteorological parameters: pressure and temperature. In a canonical case, they should be taken from sensors located near the GNSS station at the antenna height. Unfortunately, in many cases the stations are not equipped with meteorological sensors. To overcome this limitation, many studies interpolate data from nearby synoptic stations (Baltink et al., 2002; Hagemann and Bengtsson, 2003; Wang et al., 2007). Once the PWV values are obtained we can calculate the rate of change of PWV (ROP) using the formula:

$$\mathrm{ROP} = \frac{PWV_t - PWV_{t-1}}{\Delta t} \tag{12}$$

where t denotes the current epoch and Δt is the difference between two epochs expressed in minutes. ROP is expressed in mm/minute and indicates how fast PWV changed over a station. In other words, ROP at a given time is a slope at the PWV time series for a given station. A positive slope may be indicative of an onset of convection, and in conjunction with large absolute value may indicate a coming storm. Decreasing PWV (negative ROP)

results from either the displacement of moist air masses or, if the value is relatively high, the occurrence of precipitation. The ROP may be estimated epoch by epoch or using a less frequent interval. The second approach allows one to avoid noise resulting from random changes in PWV. In our analyses, we used 15-minute intervals for the ROP calculation.

Precise positioning methods, both differential and absolute, provide estimation of tropospheric delay in zenith direction alongside tropospheric gradients (Eq. (4)). It is necessary because a signal received from low elevation satellites is affected by azimuthal asymmetry of a troposphere near a station, which has to be taken into consideration. Gradients are usually estimated in two directions: north-south and east–west, using the gradient mapping function determined by the elevation of a satellite and the azimuth of a station–satellite direction. However, in meteorological applications tropospheric gradients can be used as an indicator of anisotropy of the troposphere. For example, they should indicate a direction towards a severe weather event, especially if gradients' values are uncommonly high. Thus, a reliable estimation of horizontal gradients can be helpful in the monitoring of severe weather events. Gradients are low only if the troposphere is approximately homogeneous around a station. This occurs in two cases: (a) in calm weather conditions or (b) when the current front, with axial symmetry, is passing exactly above the GNSS station.

GNSS Data and processing. In this study, we used GPS and GLONASS observations with 30-seconds resolution from the 278 GNSS stations located in Poland (Fig. 3) belonging to three different networks, namely, the state ASG-EUPOS network (the blue triangles), and two commercials networks: TPI NETpro (the green triangles) and VRSNet.pl (the red triangles). ASG-EUPOS was established in 2008 and operates under the auspices of the Head Office of Geodesy and Cartography. It consists of 103 stations located within Poland and 24 cross-border stations. TPI NETpro is a private GNSS network formed by 136 reference stations, including 121 stations in Poland and 15 cross-border stations. It has been operating since 2012. All stations are equipped with Topcon receivers and antennas. The last network, VRSNet.pl, was established in 2012 and is formed by 81 Polish and 6 cross-border stations. All equipment in this network was manufactured by Trimble. Observations from these three networks were used to create dataset with the mean spatial density of stations at the level of one station per 1120 square kilometres.

We decided to use the PPP method because it provides an absolute estimation of the position and tropospheric parameters. Also, it is used in numerous global analysis centres for GNSS processing. This method is free of network errors, which is a shortcoming characteristic of the differential approach. Furthermore, based on our previous studies, we determined that the PPP method gives reliable results in both short (Nykiel et al., 2018) and long term (Baldysz et al., 2018) PWV values.

All calculations were performed in Bernese GNSS Software version 5.2 (Dach et al., 2015) with PPP method for the position determination. In total, we reprocessed 30-second observations from 278 permanent stations using the CODE final products (Dach et al., 2018). The choice of stations participating in our study was motivated by their ability to collect both GPS and GLONASS observations. The a priori ZHD model was taken from VMF1, whereas the wet delay was estimated every 5 min using the VMF1 wet mapping function. The tropospheric gradients were estimated with a 15-minute time interval based on the Chen & Herring gradient mapping function. We applied a priori relative constraints equal to 2 mm and 0.2 mm for tropospheric delays and gradients, respectively. The ionosphere first order effect was eliminated by using the ionospheric free linear combination. Also, we modelled the second and third order of ionospheric delays. All

observations below the 5◦elevation angle were excluded from the processing. The rest were processed using the IGS14 type mean antenna model and the final solutions were expressed in the IGS14 frame. All parameters of the GNSS processing strategy are presented in Table 1.

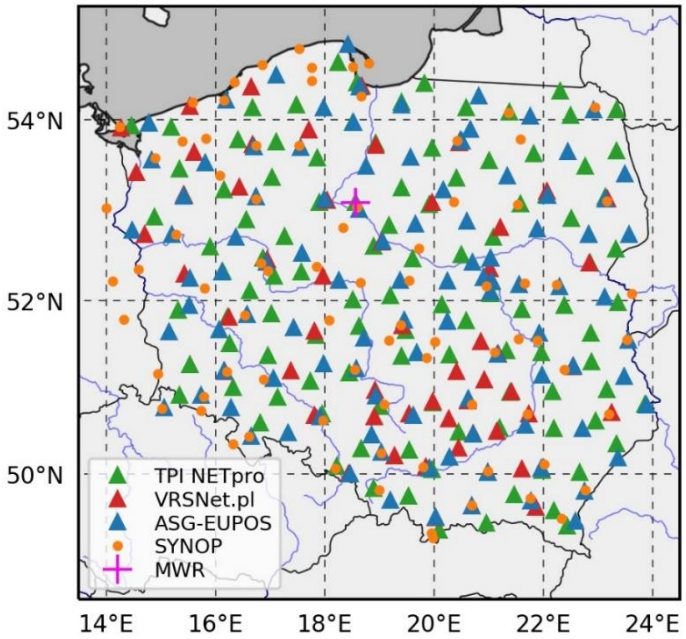

Fig. 3. Location of the GNSS stations used in the study. Stations belonging to the ASGEUPOS network are marked in blue triangles, TPI NETpro in green, and VRSNet.pl in red. The magenta cross shows a location of the microwave radiometer (MWR) and orange dots identify locations of the synoptic stations.

Table 1. GNSS processing strategy used in this study.

Data	30-sec daily RINEX from 278 GNSS stations
Satellite systems	GPS + GLONASS
Method	PPP
Software	Bernese GNSS Software ver. 5.2
A priori ZHD	VMF1
Wet tropospheric delays	Estimated with 5-min. interval using VMF1 wet mapping function. Relative constraint: 2 mm
Tropospheric gradients	Estimated with 15-min. interval using Chen and Herring mapping function. Relative constraint: 0.2 mm
Cut-off angle	5°
Ionospheric delay	1st order delay eliminated using ionospheric free linear combination; High order (2nd and 3rd) effects also included.
Orbits and clocks	CODE Final 5-min. ephemerides and 30-sec. clocks
Reference frame	IGS14
Antenna models	Type mean (IGS14)

Postprint of: Nykiel G., Figurski M., Baldysz Z., Analysis of GNSS sensed precipitable water vapour and tropospheric gradients during the derecho event in Poland of 11th August 2017, JOURNAL OF ATMOSPHERIC AND SOLAR-TERRESTRIAL PHYSICS, Vol. 193 (2019), 105082, DOI: 10.1016/j.jastp.2019.105082

For the conversion from GNSS ZTD to PWV, we used surface pressure and temperature from all available synoptic stations located in the area of the study. These are marked in Fig. 3 using orange dots. Since synoptic stations are not collocated with the GNSS, and the data interval is different (5 min for the GNSS ZWD and 1 h for the synoptic data), we had to apply time and space interpolation. First, time domain linear interpolation of sea level pressure and surface temperature for each synoptic station were performed in order to obtain the same epochs for the GNSS and meteorological parameters. Next, we performed bilinear interpolation to estimate values of meteorological parameters at the horizontal position for each GNSS station. To this end, three nearest synoptic stations were used. The median distance between GNSS and synoptic station was 25.8 km.

In case of sea level pressure (P_{sea}) we had to convert it to pressure (P) at the GNSS antenna height (h) using the surface temperature (T_s) and following formula (World Meteorological Organization, 2012):

$$P_{sea} = P \cdot \left(1 - \frac{0.0065h}{T_s + 0.0065h}\right)^{-5.257} \tag{13}$$

In the case of the temperature, we used moist adiabatic lapse rates, the typical value for which is around 0.5–0.6 K per 100 m. The median altitude difference between GNSS and synoptic station was 41.2 m.

This approach allowed deriving PWV for each station. These data were then interpolated into regular grids using bilinear interpolation. This allowed us to create the PWV and ROP maps for each epoch.

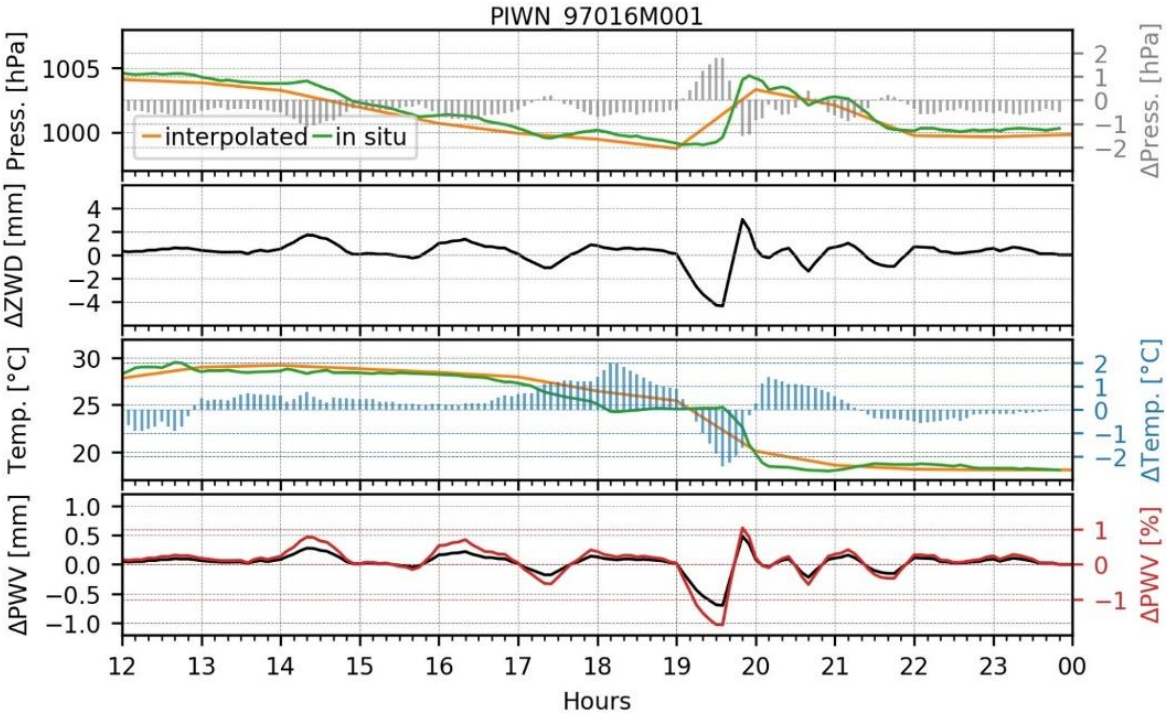

Fig. 4. Effects of the spatial and temporal interpolation of the pressure and temperature at the GNSS station PIWN. Differences between interpolated values (orange line) and those measured in-situ (green line) are presented using grey and blue bars for pressure and temperature, respectively. Moreover, the impact of the interpolation uncertainty on the ZWD and PWV parameters is presented (differences between in-situ measurements and interpolated values). The distance to the nearest synoptic station was about 21.7 km; the height difference was about 50 m.

To validate the interpolation method, we performed a comparison with the GNSS station which was equipped with the external meteorological sensor. Unfortunately, only one such station was available. Fig. 4 shows comparisons of pressure and temperature conducted for the station PIWN (Fig. 3, magenta cross). Although this station is located near the synoptic one (about 2 km), we decided not to include it in this sensitivity study. As a result, the distance between the PIWN GNSS station and the closest synoptic station was 21.7 km, and the height difference was estimated at about 50 m, which is representative for stations used in this study. Fig. 4 presents a comparison between meteorological parameters measured in-situ (with a 10-minute interval) and interpolated from synoptic stations and its effect on ZWD and PWV retrieval. Data on the synoptic stations were available every hour and thus the figure shows the influence of the spatial and temporal interpolation. Maximum differences between interpolated and in-situ meteorological parameters were about 2 hPa and 2 °C for the pressure and the temperature, respectively. The largest biases that occurred during the main phase of the derecho were caused by low temporal resolution of the synoptic data (1-hour), which was also observed for temperature just before the main event. This is caused by high spatial variability of this parameter. Under calm conditions, biases did not exceed 1 hPa and 1 °C. In Fig. 4, the impact of the interpolation errors on ZWD and the PWV parameters is also shown. It can be noticed that the maximum difference in ZWD estimation is about 4 mm and it occurs during the derecho. It stems from the uncertainties in the pressure estimation. The bias in the ZWD estimation combined with the bias in temperature estimation results in the PWV shift (according to Eq. (8) and (11)) of about 0.6 mm. However, it is small in comparison with both observed absolute values and the recorded variability (Fig. 4, bottom). This sensitivity test shows that used methodology provides a PWV estimate at a typical station with a bias much smaller than the observed amplitude of variability. Greater interpolation errors may occur in mountain areas (south part of Poland) where the difference between distance and height between GNSS and synoptic stations is bigger. However, this study focuses mainly on the event that occurred in lowland areas of Poland. Therefore, our results were not affected by the interpolation biases.

4. Results and discussions

In this section we present results of the derecho event analysis obtained from PWV and ROP maps. We also show maps of tropospheric delay gradients as indicators of intense rainfall location. Moreover, we provide two case studies of the selected GNSS stations with analysis of both PWV changes and tropospheric gradients.

PWV and ROP maps. In this subsection we first present the PWV maps obtained every 5 min based on the satellite observations from the dense network of GNSS receivers. In Fig. 5, PWV filled contour maps are shown. For easier comparison we present the same epochs as in the reflectivity analysis in Fig. 1. It can be seen that such a presentation of PWV data can provide more comprehensive information than simple scatter plots, where values for each station are shown. This results from data interpolation and is possible only if a sufficiently dense GNSS network is used. In Fig. 5, the propagation of the area of enhanced PWV values can be seen, which shows progression of the event. Initially, it was heading north-east and around 18:00 UTC it started to move northwards. The precipitation zone coincides with the area of PWV values over 40 mm. In the initial phase of the event (at 16:00 UTC) the maximum value of PWV reached 44.9 mm. Later, the front gained strength until reaching its maximum at 20:30 UTC, when the PWV value increased to 52.1 mm (presented in Fig. 5 in grey). It is worth to notice at this point that the value was more

than twice the annual average of the PWV typically measured in Poland. The strongest precipitation occurred after a clear bow echo structure had formed at around 20:00 UTC, which can be also found in the figure. It is also worth to notice that the large spatial variability in PWV was observed in the course of this phenomenon. Over a distance of about 80 km, the PWV difference reached 16.3 mm, which translates into a change of the water content in the atmosphere of approximately 0.2 kg m-2/km. It represents intensity of this phenomenon. A comparison of the data obtained from GNSS and the weather radar (Fig. 1) clearly shows them to be consistent. The area of strong precipitation, the direction and propagation velocity are all comparable. This also applies to the occurrence of the maximum PWV values and reflectivity. With an accuracy corresponding to the interval of the analysed data, the maximum values in both cases occurred at the same time (between 20:00 and 20:30 UTC). Understandably, a direct comparison of Figs. 1 and 5 gives an insight into the differences regarding the resolution of these two products. A clear bow echo structure was visible in radar images from 19:30 to 21:30 UTC, whereas in the case of the GNSS derived data a similar structure was observed only from 20:00 to 20:30 UTC. This most likely results from the fact that the resolution of the GNSS PWV is determined by the density and distribution of the GNSS stations. An increase in the number of GNSS stations would trigger a rise in the spatial resolution and therefore the quality of such maps. Nevertheless, the product presented in this article can be used to monitor the evolution of the atmospheric front.

Another product that can be obtained based on GNSS PWV is a sequence of ROP maps. They can be useful for monitoring areas characterised by rapid changes is the water vapour content in the troposphere. In Fig. 6, we present ROP maps relevant for the time of the analysed phenomenon. To ensure consistency with other datasets, we apply the 15-minute interval in the said maps. The ROP value indicates how water vapour content changes in the atmosphere. In an example presented in this study, ROP maps provide information regarding the intensification, movement and decay of the weather system. Red areas shown in Fig. 6 reflect an increase in PWV. Such a rise in the PWV content is caused by an arrival of a cold air mass that is denser than warm air. The incoming cold air mass pushes warm air underneath and creates a sloping boundary between the advancing cold air mass and the warm air mass. Consequently, warm air is forced to rise and form thicker clouds. As a result of this forced convection, a number of convective cells develop and aggregate, creating a narrow band of a heavy rainfall (Fig. 5). Oftentimes, these storms are accompanied by strong gusts of wind caused by a significant pressure difference (cold and moist air is characterised by high pressure) and downdrafts, which was also observed during this derecho. The inflow of the cold air mass into warm areas is often accompanied by rapid changes in weather with strong gradients of meteorological parameters. This is clearly seen in both Fig. 5 and Fig. 6. As we have mentioned above, the PWV content gradient reached 16.3 mm over a distance of about 100 km. The same rapid changes are also clearly visible in Fig. 6, which represents the ROP. In the analysed case, the ROP parameter reached 0.74 mm/min during the main derecho moment, around 20:00 UTC. This means that the water vapour content over the area increased very quickly, i.e. within 15 min by more than 11 mm.

Postprint of: Nykiel G., Figurski M., Baldysz Z., Analysis of GNSS sensed precipitable water vapour and tropospheric gradients during the derecho event in Poland of 11th August 2017, JOURNAL OF ATMOSPHERIC AND SOLAR-TERRESTRIAL PHYSICS, Vol. 193 (2019), 105082, DOI: 10.1016/j.jastp.2019.105082

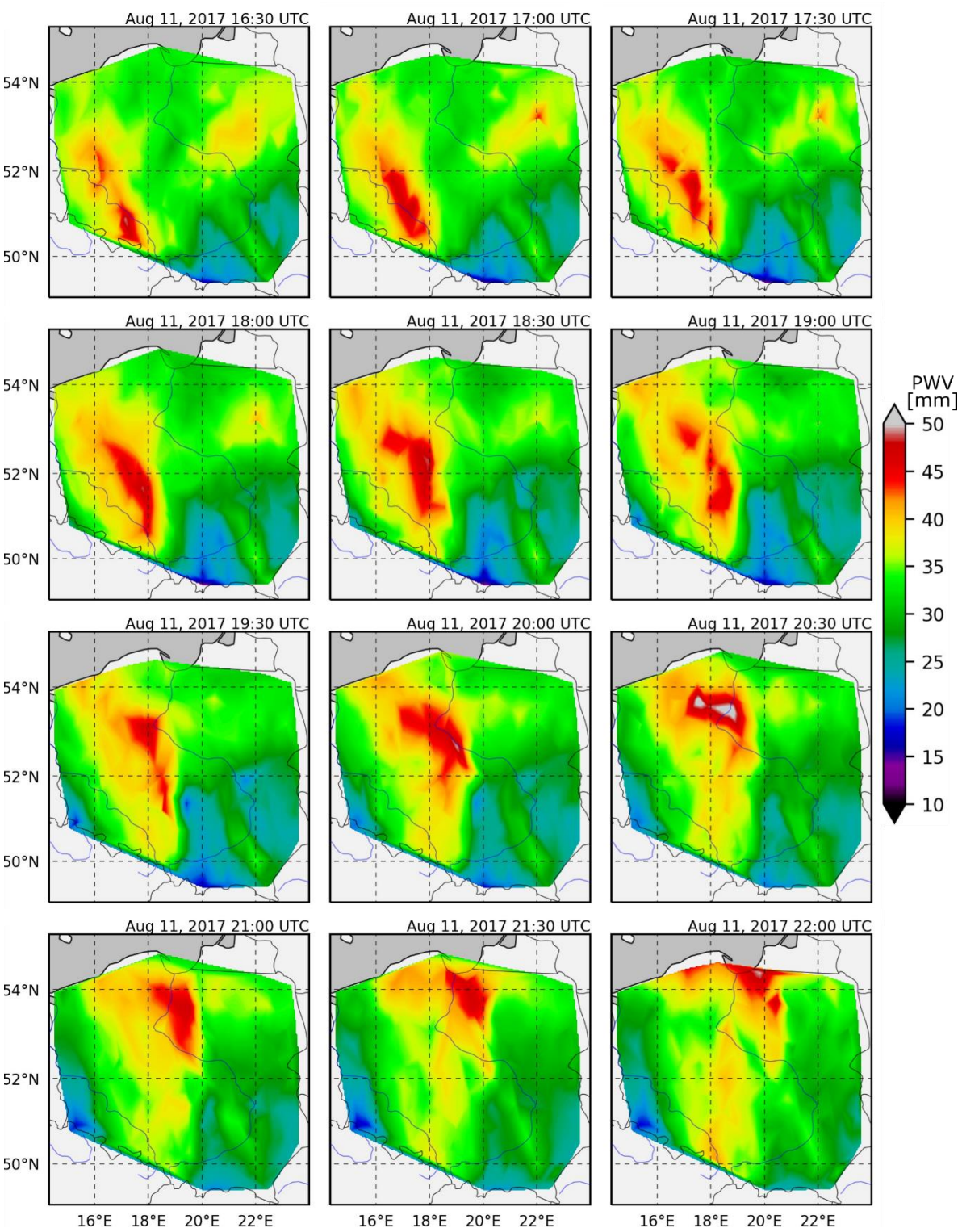

Fig. 5. PWV maps interpolated from observations from the dense network of the GNSS receivers on 11th August 2017. Results presented from 16:30 to 22:00 UTC in 30-minute steps.

Postprint of: Nykiel G., Figurski M., Baldysz Z., Analysis of GNSS sensed precipitable water vapour and tropospheric gradients during the derecho event in Poland of 11th August 2017, JOURNAL OF ATMOSPHERIC AND SOLAR-TERRESTRIAL PHYSICS, Vol. 193 (2019), 105082, DOI: 10.1016/j.jastp.2019.105082

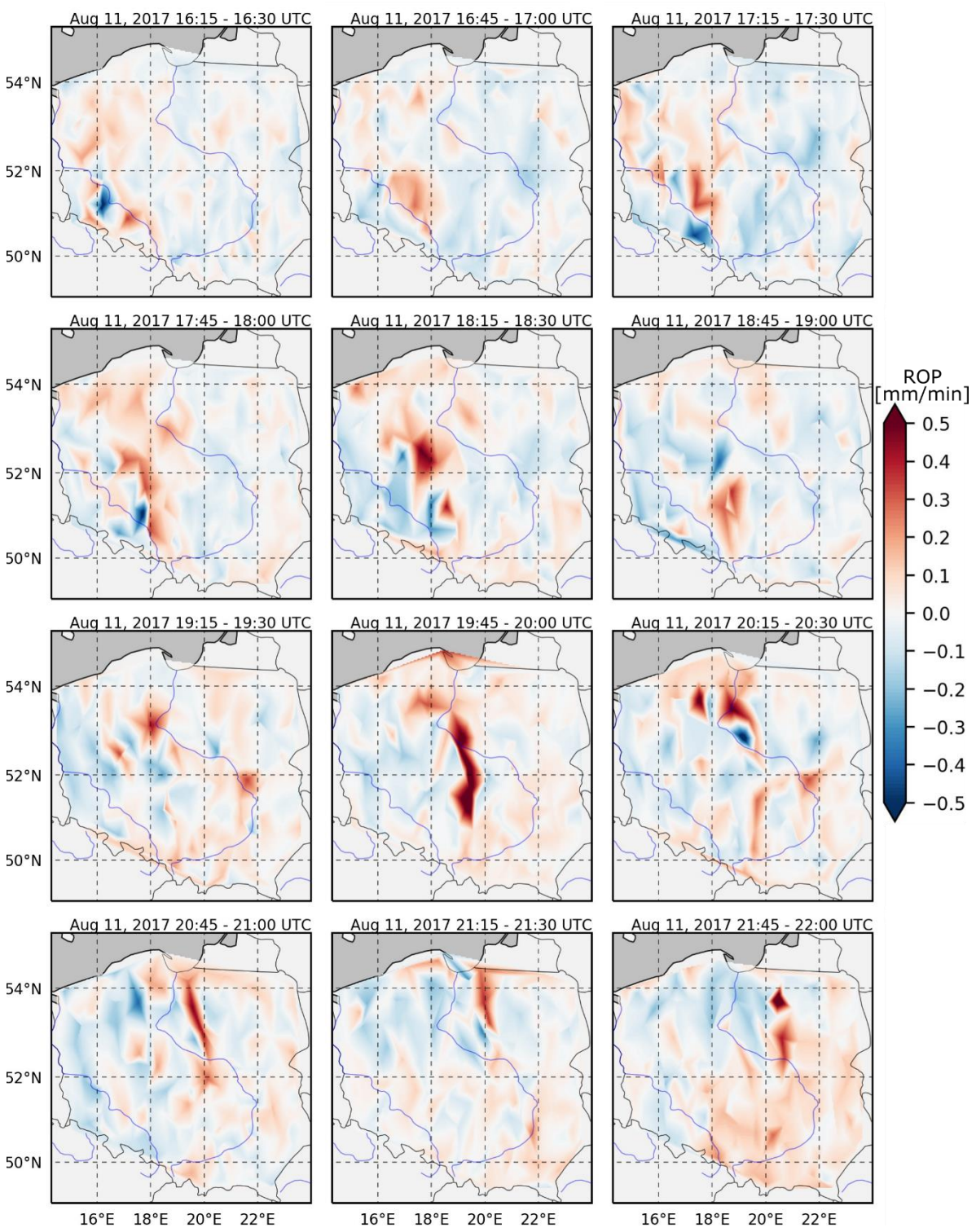

Fig. 6. ROP maps derived from the data obtained from the dense network of GNSS receivers on 11th August 2017. Results presented for the period from 16:30 to 22:00 UTC in 15-minute steps.

Fig. 6 contains also areas marked in blue that represent a decreasing ROP value. It is caused by either further movement of the front or a rainfall. The latter is clearly visible in presented results because ROP takes on a very high negative value. The minimum ROP value was observed between 20:15 and 20:30 UTC and reached −0.66 mm/min. Thus, it occurred during the main event and in addition, it corresponds to the area of strong

Postprint of: Nykiel G., Figurski M., Baldysz Z., Analysis of GNSS sensed precipitable water vapour and tropospheric gradients during the derecho event in Poland of 11th August 2017, JOURNAL OF ATMOSPHERIC AND SOLAR-TERRESTRIAL PHYSICS, Vol. 193 (2019), 105082, DOI: 10.1016/j.jastp.2019.105082

precipitation presented on the radar imagery (Fig. 1). What is more, the analysis shows that during the propagation across Poland, the system was constantly supplied with water vapour (Fig. 6). This is confirmed by the analysis of PWV maps (Fig. 5), where the maximum PWV values increased in time. Between 16:00 and 21:00 UTC an average area of ROP along the track of the system is positive. This means that the water content in the atmosphere increased epoch by epoch, which is clearly presented in Fig. 5, where the PWV value changes from 44.9 mm to 52.1 mm between 16:30 and 20:30 UTC. The intense rise is particularly evident between 19:45 and 20:00 UTC. At that time, just before the main phase of the derecho, ROP was extremely high over a large area, exceeding 0.7 mm/min. The results presented so far clearly show that both PWV and ROP maps can be very helpful in the monitoring of such severe weather events.

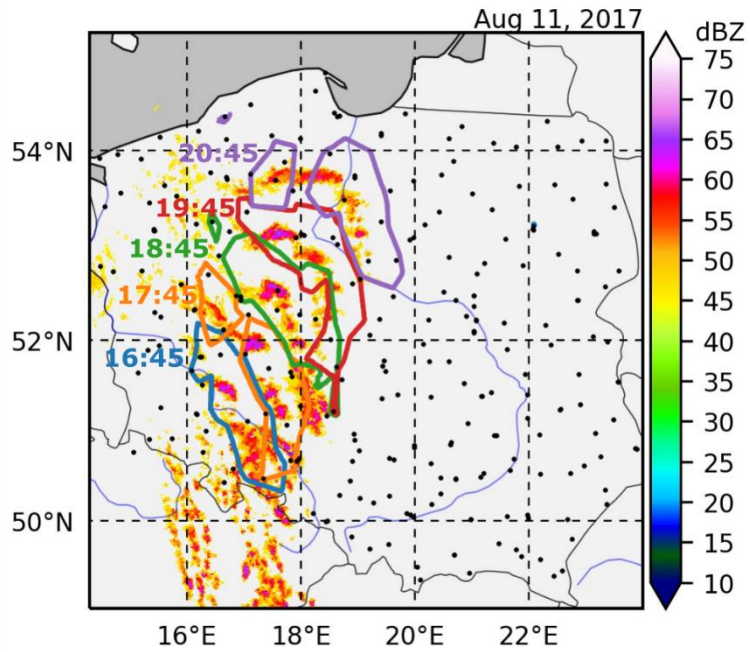

Fig. 7. Comparison of GNSS PWV with reflectivity derived from radars. Data presented for hours between 16:45 UTC (the blue line) and 20:45 UTC (the purple line) in 1-hour intervals. The outlines represent the PWV values higher than 42 mm. Reflectivity plotted only for values higher than 45 dBZ. Black dots represent the location of the GNSS stations.

In order to directly compare GNSS PWV with reflectivity, we prepared Fig. 7 that shows the combined results. In this figure, we present reflectivity data over 45 dBZ, and PWV over 42 mm high (marked by outlines). To avoid unreadable presentation of the data in the figure, we decided to show them only for a 5-hour period with a one-hour interval from 16:45 (PWV marked in blue) to 20:45 UTC (purple). However, this subset depicts well the evolution of the event and is representative for all the data in this study. It can be seen that the area where PWV is above 42 mm coincides with the area of a heavy rainfall (dBZ > 45), its size and the direction of propagation. Naturally, the selection of the presented dBZ and PWV values is arbitrary. There is no strict correlation between PWV and reflectivity absolute values, because PWV values depend on both geographic location, season of the year and local meteorological conditions. Here, it can be seen that PWV may indicate rainfall zones and that extreme PWV values also coincide with intense storms. The accuracy of the PWV maps depends mainly on the density of the GNSS stations, which determines a resolution of the final product. The only inaccuracy in the PWV data can be found at 20:45 UTC (Fig. 7, marked in purple). This is due to the lack of GNSS stations in

Postprint of: Nykiel G., Figurski M., Baldysz Z., Analysis of GNSS sensed precipitable water vapour and tropospheric gradients during the derecho event in Poland of 11th August 2017, JOURNAL OF ATMOSPHERIC AND SOLAR-TERRESTRIAL PHYSICS, Vol. 193 (2019), 105082, DOI: 10.1016/j.jastp.2019.105082

the area, causing an erroneous data interpolation. Nevertheless, by combining the estimated PWV with observations at the location of the stations one can leverage data interpretation. In this study, we used 278 GNSS stations because that is how many receivers were available at the time. However, currently there are already over 400 stations available in Poland, which would certainly improve the quality of PWV or ROP maps.

Tropospheric gradients. In this section, we present an analysis of the second tropospheric parameter obtained during the GNSS processing, namely, the tropospheric delay gradients. As we mentioned before, they can be treated as an indicator of the anisotropy of the troposphere. As in the case of the approach adopted for the PWV and ROP analyses, the data estimated at each station were interpolated into a regular grid. Examples of the obtained gradient grids are presented in Fig. 8. We show gradient values and directions (marked by black arrows) on the background of the reflectivity derived from the meteorological radars. To make the results more readable, we show only the part of Poland where the storm was the most intense.

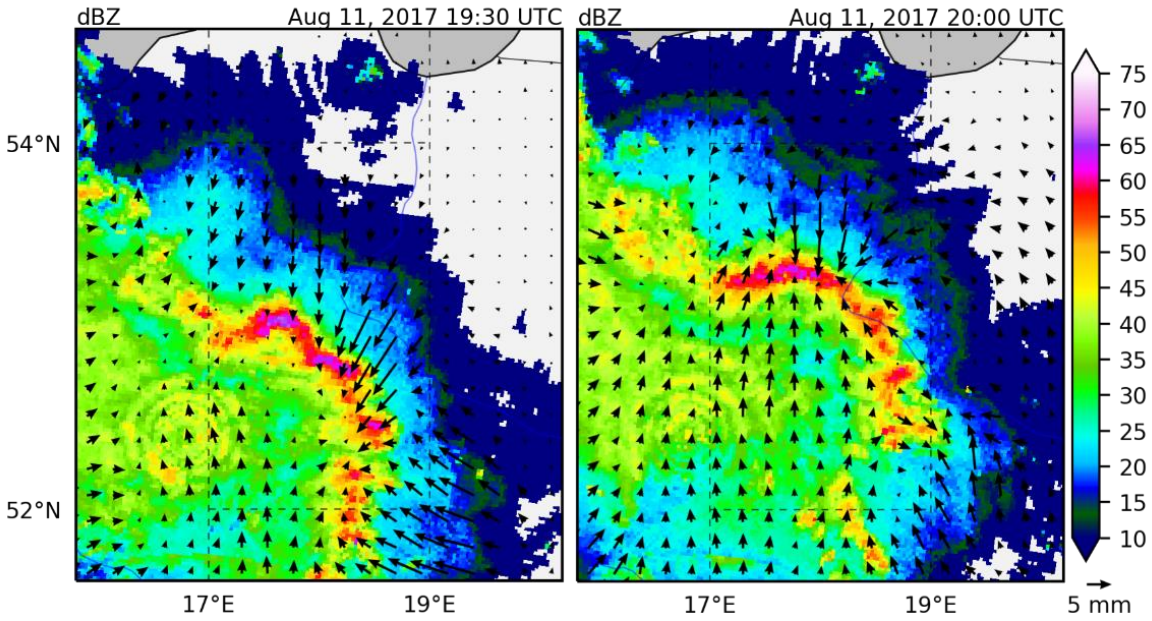

Fig. 8. Examples of the gridded gradients estimated from the GNSS observations (left: 19:30 UTC; right: 20:00 UTC) on the background of the composite reflectivity derived from the meteorological radars.

Based on results presented in Fig. 8, it can be seen that the gradient direction indicates the area characterised by the highest reflectivity. The gradient value, on the other hand, is determined by the distance from the atmospheric front. It is also clearly visible that the areas where gradients are homogeneous are limited. Such conditions are present in locations with no precipitations (the north-eastern part of the area) or directly underneath a passing front. In Fig. 8 some concentric rings with increased reflectivity values are visible (around 52.5°N and 17.0°E). However, this signal is not present in the gradient analysis and it is likely an artefact of meteorological radar data from Poznan. The results obtained from the GNSS observations are free from such errors and may serve as a verification dataset for the data obtained from meteorological radars. Likewise, the gradient data are not free from errors, unfortunately. For example, on the map representing 19:30 UTC (Fig. 8, left) not all gradient directions are appropriate in relation to the radar image. The source

Postprint of: Nykiel G., Figurski M., Baldysz Z., Analysis of GNSS sensed precipitable water vapour and tropospheric gradients during the derecho event in Poland of 11th August 2017, JOURNAL OF ATMOSPHERIC AND SOLAR-TERRESTRIAL PHYSICS, Vol. 193 (2019), 105082, DOI: 10.1016/j.jastp.2019.105082

of this bias is the same as for differences between the PWV and ROP maps (Fig. 5 and Fig. 6). In both cases, the presented maps were created based on data interpolated from the GNSS stations, which are not evenly distributed despite high density. Nevertheless, based on the presented results we can conclude that GNSS-derived tropospheric gradients can be a valuable source of data for identifying the location of propagating atmospheric fronts. This is especially important considering the fact, that the number of GNSS permanent stations is constantly increasing, thus providing a better spatial coverage.

Case study: station CHOJ. In our study we used data from 278 GNSS stations, some of which deserve a closer look. One such station is CHOJ (ASG-EUPOS network; 53.6951°N, 17.5524°E), which was the nearest station to the location of the biggest storm. This area suffered the greatest damage. Fig. 9 shows GNSS PWV time series compared to the total precipitation (the blue bars) and reflectivity (the purple line) derived from the meteorological radars (both derived from the composite data delivered by the EIG EUMETNET). The passage of moisture above the GNSS station is clearly visible. The maximum value of the PWV (52.2 mm) was observed at 20:40 UTC, while the maximum precipitation and reflectivity values (36 mm/h and 62 dBZ, respectively) were observed at 20:45 UTC. This small shift between maximum values is probably caused by the difference in temporal resolution of the data, which is 5 min for the GNSS and 15 min for the meteorological radars. Thus, it may be stated that the data from the GNSS and radars are consistent. we can also assess how fast this front was. From 16:00 to 19:45 UTC, PWV changed by about 8 mm, therefore, the average ROP was 0.03 mm/min. During the following hour, PWV changed from 36.7 mm to 52.2 mm, whereas ROP increased to the level of 0.25 mm/min. The maximum ROP value was observed between 20:15 and 20:20 UTC and it was equal to 1.08 mm/min. After the heavy rain at 20:45 UTC, the PWV value rapidly decreased over the next 15 min, dropping by about 12 mm (ROP = −0.8 mm/min). It means that the total amount of water vapour above the station decreased about 12 kg/m2. Due to precipitation, the PWV dropped to the level observed before the storm at 16:00 UTC (about 28.5 mm) over the next two hours. It should be pointed that the PWV value was growing almost steadily from 16:00 UTC until the main storm appeared in this location. It is worth to notice that the PWV value started to rapidly increase at 19:45 UTC, over half an hour before the heavy precipitation that occurred at 20:15 UTC. Thus, such information can be useful for forecasting, especially in the case of GNSS data processed online and used together with other meteorological information.

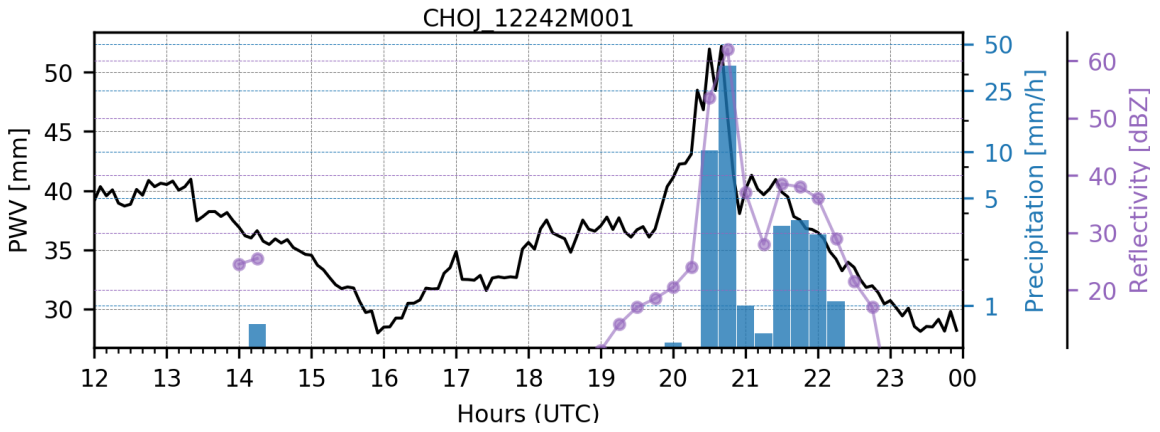

Fig. 9. GNSS PWV (the black line) estimated for the CHOJ station on 11th August 2017. The blue bars stand for precipitation derived from the radars and the purple line represents reflectivity.

Postprint of: Nykiel G., Figurski M., Baldysz Z., Analysis of GNSS sensed precipitable water vapour and tropospheric gradients during the derecho event in Poland of 11th August 2017, JOURNAL OF ATMOSPHERIC AND SOLAR-TERRESTRIAL PHYSICS, Vol. 193 (2019), 105082, DOI: 10.1016/j.jastp.2019.105082

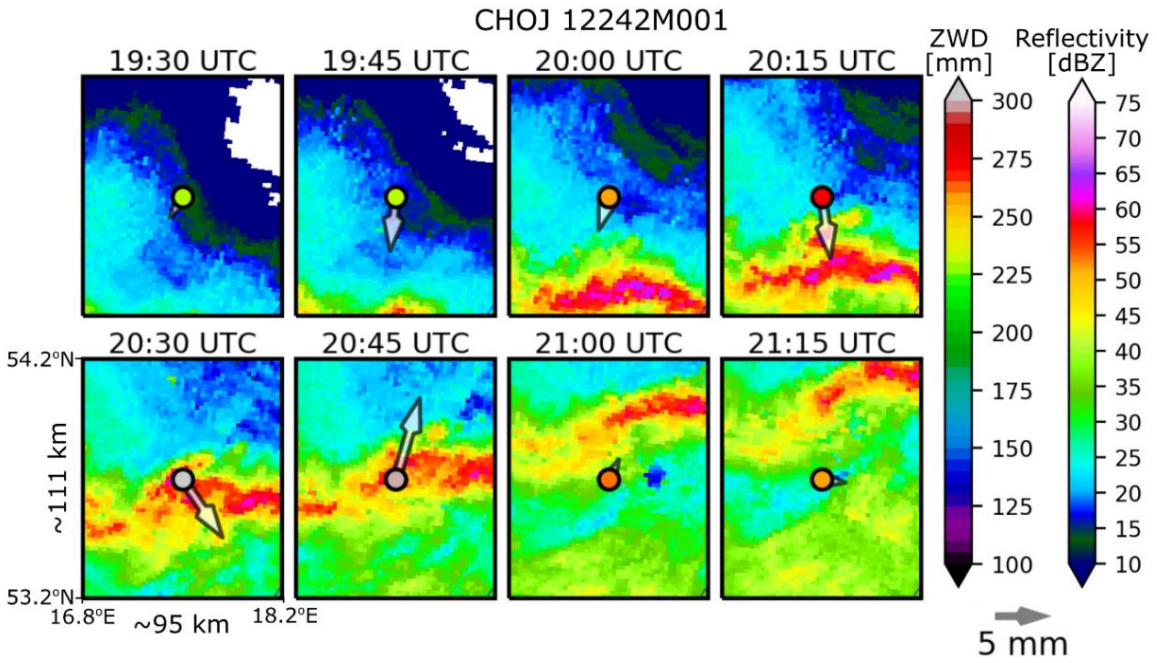

Fig. 10. Location of the CHOJ station on the background of the reflectivity data from the meteorological radars. The marker colour denotes the GNSS ZWD value estimated above the station; an arrow shows a direction and value of the maximum anisotropy of the troposphere around the station.

As we mentioned in the previous section, tropospheric gradients maps can be used as an indicator of heterogeneity of the troposphere. They can also be analysed separately for specific stations. In Fig. 10, we show the location of the CHOJ station on the background of the reflectivity derived from the meteorological radars. It is clearly seen that at 19:45 UTC, the direction of the estimated gradient directly shows the upcoming front. After the first rain occurred at 20:00 UTC (below 1 mm/h), the gradient value decreased. This was followed by a recurrent increase in the gradient value when heavy rain was approaching, showing the nearest highest value of reflectivity. During the heavy rain (between 20:30 and 20:45 UTC) the ZWD value (as well as the PWV value) was maximum. The estimated gradients show in this period a direction towards the location with higher reflectivity, where heavier precipitation occurred. During that time, the tropospheric gradients were high because the maximum reflectivity was not exactly above the station, but very close to it.

Case study: station PIWN. The second station worth additional attention is the PIWN (TPI NETpro network; 53.0953°N, 18.5602°E), which is operated by the observatory belonging to the Centre of Astronomy (Nicolaus Copernicus University in Torun, Poland) where radio-astronomical observations are performed. In August 2017 MWR (RPG HATPRO G4) was operating near this station, so we could validate the obtained GNSS PWV data. Unfortunately, the VLBI antenna could not be used because of the strong wind gusts. In Fig. 11, we show the GNSS PWV time series (the black line) as well as the PWV value from MWR (the red line), precipitation (the blue bars) and reflectivity (the purple line) measured by the meteorological radars.

Postprint of: Nykiel G., Figurski M., Baldysz Z., Analysis of GNSS sensed precipitable water vapour and tropospheric gradients during the derecho event in Poland of 11th August 2017, JOURNAL OF ATMOSPHERIC AND SOLAR-TERRESTRIAL PHYSICS, Vol. 193 (2019), 105082, DOI: 10.1016/j.jastp.2019.105082

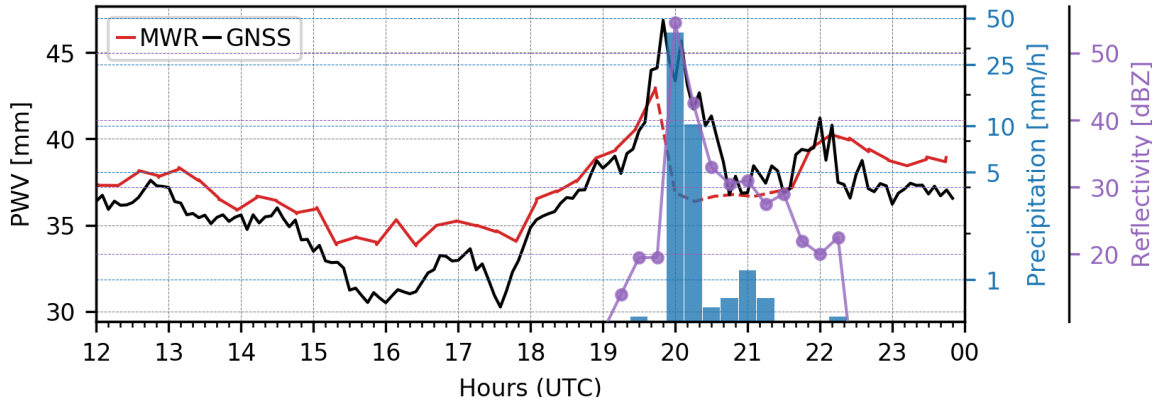

Fig. 11. PWV derived from the GNSS observations (the black line) and microwave radiometer (MWR) measurements (the red line) at PIWN station on 11th August 2017. The blue bars denote the total precipitation derived from the meteorological radars, whereas the purple line corresponds to the reflectivity measurements. The dotted red line denotes the erroneous measurements carried out with using MWR.

As in the case of the previous analysis for the CHOJ station, the consistency between GNSS PWV and reflectivity is visible. Starting from around 17:30 UTC, the PWV was increasing until 19:20 UTC (from 30.2 mm to 38.8 mm), when the storm arrived at the station. Then, a sudden increase in the PWV value occurred. Within 30 min, the value increased to 47 mm. At the same time, the ROP value was 0.27 mm/min, similar as in the case of the CHOJ station at the time of the storm arrival. After the precipitation, the PWV value dropped within 45 min from 45.6 mm to about 37 mm. As in the previous case, a small shift between peak values of the signals resulting from the data intervals can be seen. In Fig. 11, we also presented the data obtained from MWR (the red line). It can be seen that before the onset of heavy rainfall (before 19:45 UTC) the measurements from MWR are slightly larger in comparison to GNSS PWV. This may be due to one or more of the following factors: (a) improper MWR calibration, (b) retrieval algorithm implemented in MWR, (c) the accuracy of ZWD determination from the GNSS observations, (d) the accuracy of the meteorological measurements used for the ZWD GNSS to PWV conversion formula. Nevertheless, it is more important that the variability of PWV obtained from GNSS and MWR is similar before and after the storm. Larger discrepancies appeared when the storm front arrived and the measurements from the microwave radiometer became erroneous. In Fig. 11, we marked them with a red dotted line. At that time, the MWR returned information that the attenuation was 100 dB, while a moment earlier it was only 1.48 dB. It is an artefact of heavy meteorological conditions during which MWR could not perform the measurements correctly. The situation returned to normal around 21:30 UTC when reflectivity dropped to around 30 dBZ. This case shows one of the greatest advantages of the GNSS technique applied in meteorology. This method of obtaining moisture information is weather independent. Measurements can be performed both during clear skies and heavy rain conditions.

In Fig. 12, we present tropospheric gradients for the PIWN station on the background of reflectivity. The presented maps clearly show how the directions and values of the estimated gradients indicate the direction towards the approaching storm. This is especially easy to see at 19:45 UTC, when the value of the estimated gradient reached up to 15 mm and clearly pointed towards the direction of the upcoming weather front. Then, during the main phase of the storm (between 20:00 and 20:15 UTC) the estimated gradients are small, which results from the fact that the largest rainfall (higher reflectivity)

Postprint of: Nykiel G., Figurski M., Baldysz Z., Analysis of GNSS sensed precipitable water vapour and tropospheric gradients during the derecho event in Poland of 11th August 2017, JOURNAL OF ATMOSPHERIC AND SOLAR-TERRESTRIAL PHYSICS, Vol. 193 (2019), 105082, DOI: 10.1016/j.jastp.2019.105082

was exactly above the station. Finally, after the main rainfall zone moved away, the ZWD value dropped significantly to about 220 mm and the gradient indicates the direction of the receding front.

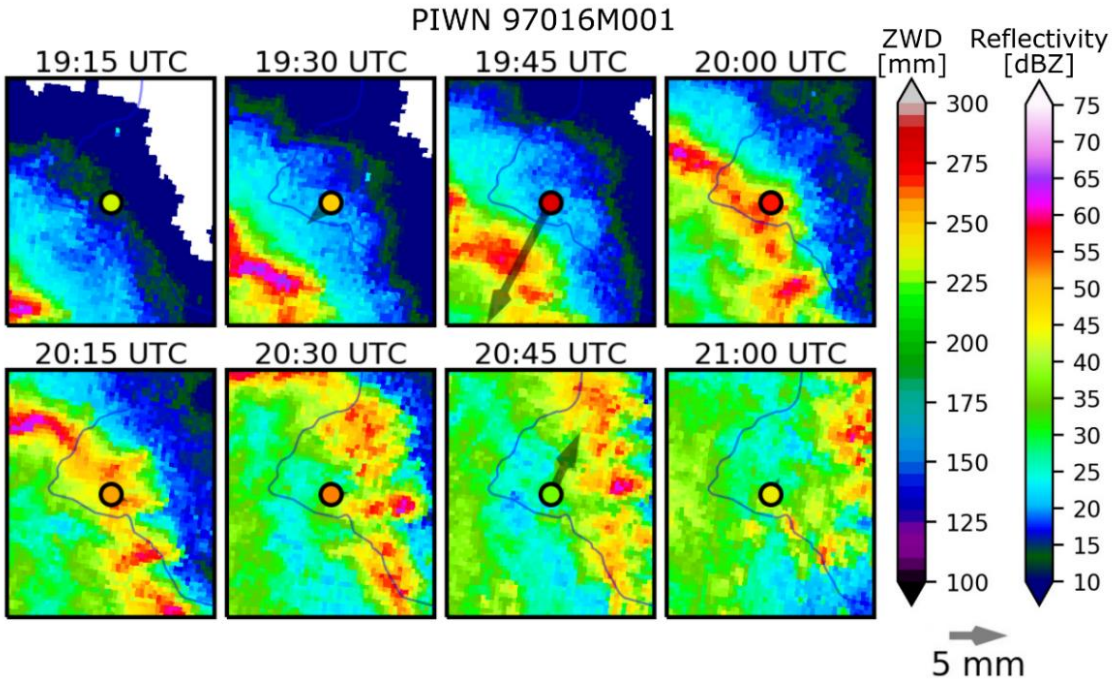

Fig. 12. The location of the PIWN station on the background of the reflectivity data from the meteorological radars. The marker colour indicates the GNSS ZWD value estimated above the station; the arrow shows the direction and value of the maximum tropospheric anisotropy.

5. Conclusions

In this paper, we presented analyses of the GNSS-sensed precipitable water vapour and the tropospheric gradients during the dangerous weather phenomena of derecho in Poland on 11th August 2017. In our analyses we used GPS/GLONASS observations from the dense network of 278 GNSS stations. These data served for estimating ZTD and tropospheric gradients with a 5 and 15-minute interval, respectively. Based on that and meteorological parameters from synoptic stations, ZTD was converted into PWV. Then high resolution PWV, ROP, and tropospheric gradients maps were created. The obtained results were compared to the composite reflectivity data derived from meteorological radars. The conducted analyses allowed us to make the following conclusions:

1. In the era of constantly developing GNSS networks, both national and commercial ones, the number of permanent stations is still growing and often exceeds the number of meteorological stations in a given region. Such a large density of GNSS stations can be used to derive PWV maps with high time and spatial resolution, even in real time. No other meteorological ground-based measurement technique gives the same opportunity. Of course, thus obtained meteorological products differ in their spatial resolution from the products obtained based on meteorological radar measurements. However, GNSS is the only technique that can provide tropospheric data, regardless of the weather conditions.
2. We obtained a strong agreement between the PWV/ROP maps and measurements from meteorological radars. The maximum values of reflectivity and atmospheric

precipitation coincided with the maximum values of GNSS PWV. This shows GNSS technique sensitivity to weather changes, which allows to use it for the monitoring of severe weather phenomena. This applies to the amount of water content in the troposphere and its rapid changes, as well as the size and direction of a movement of a weather system. The obtained results indicate that there is possibility to improve the forecasting of heavy rainfall events on the basis of ROP parameter. The rapid changes of the GNSS PWV parameter precede the occurrence of the strongest rainfall during the analysed derecho phenomenon. These results are similar with those found by Yao et al. (2017).

3. The accuracy and reliability of the maps presented in this article depend on the density and placement of GNSS stations. We used data from 278 stations, while at present there are over 400 stations available in Poland, which definitely increases the quality of data and their possible interpretation. We realise that such a situation is not present in every country, which leaves a need for new solutions. One of them may be, for example, the use of low-cost single-frequency receivers that can be used to increase density of the existing networks. The tropospheric data currently obtained on this basis are starting to be comparable to those obtained with a dual frequency receiver (Barindelli et al., 2018; Krietemeyer et al., 2018).
4. A tropospheric gradient maps can be a valuable source of information about the location and size of upcoming extreme weather events owing to the sensitivity of GNSS gradients to changes in the troposphere anisotropy. Therefore, they can be used not only to monitor the current location of the storm but also potentially in forecasting, e.g. as a contribution to the numerical weather model (Zus et al., 2019). As in the case of the PWV/ROP maps, their credibility is strictly related to the density of GNSS stations.
5. It should be noted that tropospheric gradients have a limited range, which results from the number of visible satellites and the path of their signals passing through the troposphere. We can expect that the best results would be obtained with the satellites evenly distributed across the sky in the function of both the azimuth and elevation angles. This would give most reliable results, while gradients could indicate the fronts at a distance up to 100 km (assuming a 5◦ elevation mask and a troposphere height of 10 km). Therefore, it seems important that the largest possible number of satellite systems is used. We intend to conduct further research in this area. Based on currently published findings (Baldysz et al., 2017), we can already state that the selection of constellations can have an impact on the values and directions of the gradients.

Acknowledgements

The Authors would like to thank the institutions and companies for granting access to the observational data, namely, the Polish Head Office of Geodesy and Cartography for the data from the ASG-EUPOS, the TPI company for sharing data from TPI NETpro network, and VRSNet company for sharing data from their network. The Authors would like to thank the EIG EUMETNET for providing composite reflectivity and precipitation data from meteorological radars. Calculations were carried out at the Academic Computer Centre in Gdansk. Special thanks to Dariusz Baranowski, Ph.D. for valuable insights. The Authors would also like to acknowledge the contribution of the COST Action ES1206.

References

Baldysz, Z., Nykiel, G., Araszkiewicz, A., Figurski, M., Szafranek, K., 2016. Comparison of GPS tropospheric delays derived from two consecutive EPN reprocessing campaigns from the point of view of climate monitoring. Atmos. Meas. Tech. 9, 4861–4877. http://dx.doi.org/10.5194/amt-9-4861-2016.

Baldysz, Z., Nykiel, G., Figurski, M., Araszkiewicz, A., 2018. Assessment of the impact of GNSS processing strategies on the long-term parameters of 20 years IWV time series. Remote Sens. 10 (4), 496. http://dx.doi.org/10.3390/rs10040496.

Baldysz, Z., Szolucha, M., Nykiel, G., Figurski, M., 2017. Analysis of the impact of Galileo observations on the tropospheric delays estimation. In: 2017 Baltic Geodetic Congress (BGC Geomatics). pp. 65–71. http://dx.doi.org/10.1109/BGC.Geomatics.2017.22.

Baltink, H., van der Marel, H., Hoeven, A., 2002. Integrated atmospheric water vapor estimates from a regional GPS network. J. Geophys. Res. (D3), http://dx.doi.org/10.1029/2000JD000094.

Barindelli, S., Realini, E., Venuti, G., Fermi, A., Gatti, A., 2018. Detection of water vapor time variations associated with heavy rain in northern Italy by geodetic and low-cost GNSS receivers. Earth Planets Space 70 (28), http://dx.doi.org/10.1186/s40623-018-0795-7.

Benevides, P., Catalao, J., Miranda, P., 2015. On the inclusion of GPS precipitable water vapour in the nowcasting of rainfall. Nat. Hazards Earth Syst. Sci. 15, 2605–2616. http://dx.doi.org/10.5194/nhess-15-2605-2015.

Bevis, M., Businger, S., Chiswell, S., Herring, T., Anthes, R., Rocken, C., Ware, R., 1994. GPS meteorology: Mapping zenith wet delays onto precipitable water. J. Appl. Meteorology Climatol. 33, 379–386. http://dx.doi.org/10.1175/1520-0450(1994)033<0379:GMMZWD>2.0.CO;2.

Bevis, M., Businger, S., Hering, T., Rocken, C., Anthes, R., Ware, R., 1992. GPS meteorology: Remote sensing o atmospheric water vapour using the global positioning system. J. Geophys. Res. 97, 15787–15801. http://dx.doi.org/10.1029/92JD01517.

Boehm, J., Niell, A., Tregoning, P., Schuh, H., 2006a. Global mapping function (GMF): A new empirical mapping function based on numerical weather model data. Geophys. Res. Lett. 33.

Boehm, J., Werl, B., Schuh, H., 2006b. Troposphere mapping functions for GPS and very long baseline interferometry from European centre for medium-range weather forecasts operational analysis data. J. Geophys. Res. 111.

Brenot, H., Neméghaire, J., Delobbe, L., Clerbaux, N., De Meutter, P., Deckmyn, A., Delcloo, A., Frappez, L., Van Roozendael, M., 2013. Preliminary signs of the initiation of deep convection by GNSS. Atmos. Chem. Phys. 13, 5425–5449. http://dx.doi.org/10.5194/acp-13-5425-2013.

Chen, G., Herring, A., 1997. Effects of atmospheric azimuthal asymmetry on the analysis of space geodetic data. J. Geophys. Res. 102, 20489–20502. http://dx.doi.org/10.1029/97JB01739.

Choy, C., Wanga, C., Zhanga, K., Kuleshovab, Y., 2013. GPS sensing of precipitable water vapour during the March 2010 Melbourne storm. Adv. Space Res. 52 (9), http://dx.doi.org/10.1016/j.asr.2013.08.004.

Copernicus Climate Change Service (C3S), 2017. ERA5: Fifth generation of ECMWF atmospheric reanalyses of the global climate. In: Copernicus Climate Change Service Climate Data Store (CDS). https://confluence.ecmwf.int/display/CKB/ERA5+data+documentation.

Cornwall, W., 2016. Efforts to link climate change to severe weather gain ground. Science 351 (6279), 1249–1250. http://dx.doi.org/10.1126/science.351.6279.1249.

Dach, R., Lutz, S., Walser, P., Fridez, P., 2015. Bernese GNSS software version 5.2. In: User Manual. Astronomical Institute, University of Bern.

Dach, R., Schaer, S., Arnold, D., Prange, L., Sidorov, D., Stebler, P., Villiger, A., Jäggi, A., 2018. CODE final product series for the IGS. Astronomical Institute, University of Bern, http://dx.doi.org/10.7892/boris.75876.3.

Davis, J., Herring, T., Shapiro, I., Rogers, E., Elgered, G., 1985. Geodesy by radio interferometry: Effects of atmospheric modeling errors on estimates of baseline length. Radio Sci. 20, 1593–1607. http://dx.doi.org/10.1029/RS020i006p01593.

Faccani, C., Ferretia, R., Pacione, R., Paolucci, T., Vespe, F., Cucurull, L., 2005. Impact of a high density GPS network on the operational forecast. Adv. Geosci. 2, 73–79.

Field, C., Barros, V., Stocker, T., Qin, D., Dokken, D., Ebi, K., Mastrandrea, M., Mach, K., Plattner, G., Allen, S., Tignor, M., Midgley, P., 2012. Managing the risks of extreme events and disasters to advance climate change adaptation. In: A Special Report of Working Groups I and II of the Intergovernmental Panel on Climate Change. Cambridge University Press, NY, USA, https://www.ipcc.ch/pdf/specialreports/srex/SREX_Full_Report.pdf.

Gradinarsky, L., Johansson, J., Bouma, H., Scherneck, H., Elgered, G., 2002. Climate monitoring using GPS. Phys. Chem. Earth 27, 335–340. http://dx.doi.org/10.1016/S1474-7065(02)00009-8.

Guerova, G., Jones, J., Dousa, J., Dick, G., de Haan, S., Pottiaux, E., Bock, O., Pacione, R., Elgered, G., Vedel, H., Bender, M., 2016. Review of the state of the art and future prospects of the ground-based GNSS meteorology in Europe. Atmos. Meas. Tech. 9 (11), http://dx.doi.org/10.5194/amt-9-5385-2016.

Hagemann, S., Bengtsson, L., 2003. On the determination of atmospheric water vapor from GPS measurements. J. Geophys. Res. 108, http://dx.doi.org/10.1029/2002JD003235.

Herring, T., Bengtsson, L., Gendt, G., 1992. On the determination of atmospheric water vapor from GPS measurements. Radio Sci. 108, 157–164. http://dx.doi.org/10.1029/2002JD003235.

Herring, S.C., Christidis, N., Hoell, A., Kossin, J.P., Schreck, C.J., Stott, P.A., 2018. Explaining extreme events of 2016 from a climate perspective. Bull. Am. Meteorol. Soc. 99 (1), S1–S157. http://dx.doi.org/10.1175/BAMSExplainingExtremeEvents2016.1.

Kehrer, K., Graf, B., Roeder, W., 2008. Global positioning system (GPS) precipitable water in forecasting lightning at spaceport Canaveral. Weather Forecast 23, 219–232. http://dx.doi.org/10.1175/2007WAF2006105.1.

Krietemeyer, A., ten Veldhuis, M., van der Marel, H., Realini, E., van de Giesen, N., 2018. Potential of cost-efficient single frequency GNSS receivers for water vapor monitoring. Remote Sens. 10, http://dx.doi.org/10.3390/rs10091493.

LaDue, D., Heinselman, P., Newman, J., 2009. Strengths and limitations of current radar systems for two stakeholder groups in the southern plains. American Meteorological Society http://dx.doi.org/10.1175/2009BAMS2830.1.

Mazany, R., Businger, S., Gutman, S., 2002. A lightning prediction index that utilizes GPS integrated precipitable water vapor. Weather Forecast 17, 1034–1047. http://dx.doi.org/10.1175/1520-0434(2002)017<1034:ALPITU>2.0.CO;2.

Nilsson, T., Elgered, G., 2008. Long-term trends in the atmospheric water vapor content estimated from ground-based GPS data. J. Geophys. Res. 113 (D19101), http://dx.doi.org/10.1029/2008JD010110.

Ning, T., Elgered, G., 2012. Trends in the atmospheric water vapor content from ground-based GPS: The impact of the elevation cut off angle. IEEE J. Sel. Top. Appl. 5, 744–751. http://dx.doi.org/10.1109/JSTARS.2012.2191392.

Nykiel, G., Wolak, P., Figurski, M., 2018. Atmospheric opacity estimation based on IWV derived from GNSS observations for VLBI applications. GPS Solut. 22 (9), http://dx.doi.org/10.1007/s10291-017-0675-9.

Pacione, R., Sciarretta, C., Faccani, F.V.C., R. Ferretti, R., Fionda, E., Ferraro, C., Nardi, A., 2001. GPS meteorology: Validation and comparisons with ground-based microwave radiometer and mesoscale model for the Italian GPS permanent stations. Phys. Chem. Earth 26, 139–145. http://dx.doi.org/10.1016/S1464-1895(01)00037-0.

Powers, J.G., Klemp, J.B., Skamarock, W.C., Davis, C.A., Dudhia, J., Gill, D.O., Coen, J.L., Gochis, D.J., Ahmadov, R., Peckham, S.E., Grell, G.A., Michalakes, J., Trahan, S., Benjamin, S.G., Alexander, C.R., Dimego, G.J., Wang, W., Schwartz, C.S., Romine, G.S., Liu, Z., Snyder, C., Chen, F., Barlage, M.J., Yu, W., Duda, M.G., 2017. The weather research and forecasting model: Overview, system efforts, and future directions. Bull. Am. Meteorol. Soc. 98 (8), 1717–1737. http://dx.doi.org/10.1175/BAMS-D-15-00308.1.

Qingzhi, Z., Yibin, Y., Wangiang, Y., 2018. GPS-based PWV for precipitation forecasting and its application to a typhoon event. J. Atmos. Sol.-Terr. Phys. 167, 124–133. http://dx.doi.org/10.1016/j.jastp.2017.11.013.

Randall, D., 2000. General Circulation Model Development. Academic Press.

Ruger, J., 2002. Refractive Index Formulae for Radio Waves. In: Proceedings of the FIG XXII International Congress.

Saastamoinen, J., 1972. Atmospheric correction for the troposphere and stratosphere in ranging satellites. In: The Use of Artificial Satellites for Geodesy, Geophysical Monography No. 15. American Geophysical Union, pp. 247–251.

Seidel, D., Sun, B., Pettey, M., Reale, A., 2011. Global radiosonde balloon drift statistics. J. Geophys. Res. 116, http://dx.doi.org/10.1029/2010JD014891.

Seko, H., Shimada, S., Nakamura, H., Kato, T., 2000. Three dimensional distribution of water vapor estimated from tropospheric delay of GPS data in a mesoscale precipitation system of the baiu front. Earth Planets Space 52, 927–933. http://dx.doi.org/10.1186/BF03352307.

Suparta, W., Ali, M., 2014. Nowcasting the lightning activity in Peninsular Malaysia using the GPS PWV during the 2009 inter-monsoons. Ann. Geophys. 57, http://dx.doi.org/10.4401/ag-6373.

Vedel, H., Huang, X.-Y., Haase, J., Ge, M., Calais, E., 2004. Impact of GPS zenith tropospheric delay data on precipitation forecasts in Mediterranean France and Spain. Geophys. Res. Lett. 31 (2), http://dx.doi.org/10.1029/2003GL017715.

Wang, J., Zhang, L., Dai, A., Van Hove, T., Van Baelen, J., 2007. A near-global, 2-hourly data set of atmospheric precipitable water from ground-based GPS measurements. J. Geophys. Res. 112, http://dx.doi.org/10.1029/2006JD007529.

Widawski, A., Pilorz, W., 2018. The mesoscale convective systems with bow echo radar signatures as an example of extremely severe and widespread geohazard in Poland. Socio.-econ. Stud. 6 (1), 10–16. http://dx.doi.org/10.2478/environ-2018-0002.

World Meteorological Organization, 2012. CIMO/ET-Stand-1/Doc. 10, pressure reduction formula. https://www.wmo.int/pages/prog/www/IMOP/meetings/SI/ETStand-1/Doc-10_Pressure-red.pdf.

Yao, Y., Shan, L., Zhao, Q., 2017. Establishing a method of short-term rainfall forecasting based on GNSS-derived PWV and its application. Sci. Rep. 7.

Zhang, M., Ni, Y., Zhang, F., 2007. Variational assimilation of GPS precipitable water vapor and hourly rainfall observations for a mesoscale heavy precipitation event during the 2002 Mei-Yu season. Adv. Atmos. Sci. 24, 509–526. http://dx.doi.org/10.1007/s00376-007-0509-8.

Zhao, Q., Yao, Y., Yao, W., 2018. GPS-based PWV for precipitation forecasting and its application to a typhoon event. J. Atmos. Sol.-Terr. Phys. 167, 124–133. http://dx.doi.org/10.1016/j.jastp.2017.11.013.

Zus, F., Dousa, J., Kacmarik, M., Vaclavovic, P., Dick, G., Wickert, J., 2019. Estimating the impact of global navigation satellite system horizontal delay gradients in variational data assimilation. Remote Sens. 10 (4), 496. http://dx.doi.org/10.3390/rs11010041.